Ab Initio Atomistic Thermodynamics for Surfaces: A Primer

Jutta Rogal and Karsten Reuter
Fritz-Haber-Institut der Max-Planck-Gesellschaft
Faradayweg 4-6
D-14195 Berlin
Germany

reuter@fhi-berlin.mpg.de

1.0 INTRODUCTION

Rational design and advancement in materials science will ultimately rely on an atomic-scale understanding of the targeted functionality. Corresponding modeling must then address the behavior of electrons and the resulting interactions (often expressed in the terminology of chemical bonds) that govern the elementary processes among the atoms and molecules in the system. Modern electronic structure theory methods like density-functional theory (DFT) [1-5] have matured to a standard tool for this task, allowing a description that is often already accurate enough to allow for a modeling with predictive character. These techniques are referred to as first-principles (or in latin: *ab initio*) to indicate that they do not rely on empirical or fitted parameters, which then makes them applicable for a wide range of realistic conditions, e.g. realistic environmental situations of varying temperatures and pressures [6].

The latter type of application seems at first sight at variance with the frequent argument describing DFT as a zero-temperature, zero-pressure technique. Such a confusion arises, when thinking that DFT provides (apart from a wealth of information about the electronic structure) "only" the total energy of the system. Instead, it is crucial to realize that this kind of energetic information can be obtained as a function of the atomic configuration $\{\mathbf{R}_I\}$. This leads to the so-called potential energy surface (PES) $E(\{\mathbf{R}_I\})$, which then contains the relevant information needed to describe the effect of temperature on the atomic positions. Obviously, a (meta)stable atomic configuration corresponds to a (local) minimum of the PES. The forces acting on the given atomic configuration are just the local gradient of the PES, and the vibrational modes of a (local) minimum are given by the local PES curvature around it.

One possibility to go from this to situations of finite temperature and finite pressure is to achieve a matching with thermodynamics. This is the general idea behind *ab initio* atomistic thermodynamics, namely to employ the information on the first-principles PES to calculate appropriate thermodynamic potential functions like the Gibbs free energy [7-10]. Once such a quantity is known, one is immediately in a position to evaluate macroscopic system properties using the standard methodology of thermodynamics. Apart from bridging to any (T,p)-conditions, this methodology is particularly useful for larger systems, which may readily be divided into smaller subsystems that are mutually in equilibrium with each other. Each of the smaller and thus potentially simpler subsystems can then be first treated separately, and the contact between the subsystems is thereafter established by relating their corresponding thermodynamic potentials. Such a "divide and conquer" type of approach can be especially efficient, if infinite, but homogeneous parts of the system like bulk or surrounding gas phase can be separated off, and are then merely represented by corresponding reservoirs [11-16]. Although not further discussed here, another aspect could be to consider situations of "constrained equilibria" [14,15], where not all, but only some of the subsystems are in thermodynamic equilibrium.

Rogal, J.; Reuter, K. (2007) *Ab Initio* Atomistic Thermodynamics for Surfaces: A Primer. In *Experiment, Modeling and Simulation of Gas-Surface Interactions for Reactive Flows in Hypersonic Flights* (pp. 2-1 – 2-18). Educational Notes RTO-EN-AVT-142, Paper 2. Neuilly-sur-Seine, France: RTO. Available from: http://www.rto.nato.int/abstracts.asp.

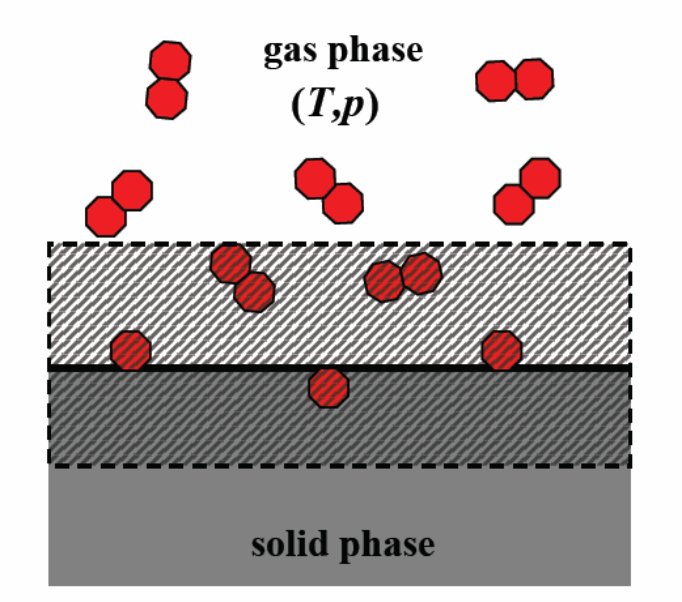

Figure 1: Schematic representation of the system discussed here, a single-crystal metal surface in contact with a surrounding gas phase characterized by defined temperature *T* and pressure *p*. The shaded area represents the finite part of the system that is affected by the presence of the surface.

2.0 SURFACES IN REALISTIC ENVIRONMENTS

2.1 Surface free energy

Here we will illustrate how this quite general concept works and what it can contribute in practice by using it to determine the equilibrium geometry and composition of a solid surface in contact with a given environment at finite temperature and pressure. For the sake of simplicity we consider the case of a monoatomic metal and an oxygen atmosphere described by an oxygen pressure p and a temperature T [17-20], and refer to the literature for the generalizations to compounds like oxides [13] or alloys [21], and to environments containing multiple gas phase species [14,15]. Under conditions of defined (T,p), the appropriate thermodynamic potential to consider is the Gibbs free energy. For this quantity we introduce the following notation: Capital G refers to an absolute Gibbs free energy, while lower case g is used to denote a Gibbs free energy per formula unit or particle. In the case of an infinite, homogeneous system the latter is then equivalent to the chemical potential μ, i.e. if the homogeneous system is viewed as a reservoir, μ gives the cost at which this reservoir provides particles. For convenience we will use the symbol μ instead of g, when we want to emphasize a system's role as a reservoir. In the present context it is particularly the oxygen environment which acts as such a reservoir, because it can give (or take) any amount of oxygen to (or from) the sample without changing the temperature or pressure.

Figure 1 shows a schematic representation of the system discussed here, a solid phase in contact with a surrounding gas phase. We can break down the Gibbs free energy of this entire system into contributions coming from the bulk of the solid phase G_{solid}, from the homogeneous gas phase G_{gas} and an additional term introduced through the surface ΔG_{surf}

(1) $$G = G_{solid} + G_{gas} + \Delta G_{surf} \quad .$$

If the surface is homogeneous as in the case of an ideal single-crystal surface, ΔG_{surf} will scale linearly with the surface area A, and we can introduce the surface free energy per unit area, γ. Upon rearranging eq. (1) we therefore have

$$(2) \qquad \gamma = \frac{1}{A}\left(G - G_{solid} - G_{gas}\right) \quad .$$

We notice that γ is well defined by a finite part of the total (infinite) system. With increasing distance from the surface, eventually both the solid and the gas phase part of the total system will no longer be affected by the created surface. Although contained in G, these (infinite) parts of the total system are then effectively canceled out in eq. (2) by the subtraction of the equivalent amounts of homogeneous systems (G_{gas} and G_{solid}). We can therefore concentrate on the finite part of the system that is affected by the surface. If this part contains N_M metal atoms and N_O oxygen atoms per surface area, this allows us to rewrite eq. (2) as

$$(3) \qquad \gamma(T,p) = \frac{1}{A}\left(G(T,p,N_O,N_M) - N_M g_M(T,p) - N_O \mu_O(T,p)\right) \quad ,$$

where we have introduced the Gibbs free energy per metal atom g_M in the bulk, and the oxygen chemical potential μ_O of the gas phase.

At this stage it is appropriate to spend a few words on the sign convention. In this text, a more negative Gibbs free energy will indicate a more stable state of the system. In the interpretation of a chemical potential this translates to μ approaching -∞ in the limit of an infinitely dilute gas, since adding a particle will then yield an infinite gain in entropy. As a consequence, $\gamma > 0$ indicates the cost of creating the surface between the solid bulk phase and the homogeneous gas phase. Alternatively, when discussing the stability of phases that result from adsorbing species at the solid surface, it can be convenient to choose another zero reference. Instead of γ as a measure of the cost of creating the surface at all, one can introduce the surface free energy of the clean surface

$$(4) \qquad \gamma_{clean}(T,p) = \frac{1}{A}\left(G(T,p,0,N_M) - N_M g_M(T,p)\right)$$

and evaluate the Gibbs free energy of adsorption as a measure of the cost with respect to the clean surface [17,19,20]

$$(5) \qquad \begin{aligned} \Delta G^{ad}(T,p) &= \gamma_{clean}(T,p,0,N'_M) - \gamma(T,p,N_O,N_M) = \\ &= \frac{1}{A}\left(G(T,p,N_O,N_M) - G(T,p,0,N'_M) - N_O\mu_O(T,p) - (N_M - N'_M)g_M(T,p)\right) \end{aligned} \quad ,$$

where the last term accounts for a possible difference in the number of metals atoms between the reference clean surface and the oxidized surface structural model. Obviously, the most stable surface structure and composition at given (T,p) in the gas phase is the one that minimizes the surface free energy, or equivalently the one that leads to the most positive Gibbs free energy of adsorption at the corresponding oxygen chemical potential.

2.2 Calculating Gibbs free energies

As apparent from eqs. (3) and (5) the quantities determining γ or ΔG^{ad} are the Gibbs free energy of the solid surface and of the solid bulk, as well as the chemical potential of the oxygen environment. Since the

contributions to free energies in the gas phase and in the solid phase are quite different, we will discuss the evaluation of these quantities separately. First we concentrate on the oxygen chemical potential, and then on the computation of the solid phase Gibbs free energies.

2.2.1 Gas phase chemical potential

The chemical potential of oxygen, which enters eqs. (3) and (5), is determined by the condition of thermodynamic equilibrium with the surrounding gas phase reservoir. At the accuracy level relevant for our purposes, this gas is well described by ideal gas laws. If we write the chemical potential at given temperature T and pressure p as

$$\mu_O(T,p) = \tfrac{1}{2}\,\mu_{O_2(gas)}(T,p) = \tfrac{1}{2}\left(-k_B T \ln Q^{tot}_{O_2(gas)} + pV\right)/N \quad , \tag{6}$$

we therefore have to evaluate the partition function $Q^{tot}_{O_2(gas)}$ of an ideal gas composed of N indistinguishable O_2 molecules

$$Q^{tot}_{O_2(gas)} = \frac{1}{N!}\left(q_{O_2}\right)^N = \frac{1}{N!}\left(q^{trans} q^{rot} q^{vib} q^{electr} q^{nucl}\right)^N \tag{7}$$

with q_{O_2} the partition function of one O_2 molecule, which can further be subdivided into different partition functions with obvious nomenclature. In writing eq. (7) we assumed that the nuclear/electronic (nucl, electr) degrees of freedom are decoupled from the vibrational/rotational (vib, rot) ones (Born-Oppenheimer approximation), and further that also vibrational and rotational motions are decoupled as they take place on different time scales.

Inserting eq. (7) into eq. (6) we then arrive at

$$\mu_O(T,p) = -\frac{1}{2N}\left[k_B T \ln\left(\frac{1}{N!}(q^{trans})^N\right) - pV\right] + \tfrac{1}{2}\mu^{rot} + \tfrac{1}{2}\mu^{vib} + \tfrac{1}{2}\mu^{electr} + \tfrac{1}{2}\mu^{nucl} \quad , \tag{8}$$

and proceed here by briefly commenting on the translational, rotational, vibrational, electronic and nuclear free energy terms. A more detailed derivation can be found in most textbooks on Statistical Mechanics, e.g. the one by Mc Quarrie [22].

Translational free energy

In the classical limit the energy due to the center-of-mass motion of a particle in a box is

$$\varepsilon_{\mathbf{k}} = \frac{\hbar^2 \mathbf{k}^2}{2m} \quad , \qquad \mathbf{k} = \frac{\pi}{L}\left(n_x \hat{x} + n_y \hat{y} + n_z \hat{z}\right) , \tag{9}$$

where $L = V^{1/3}$ characterizes the box size, m is the mass of one particle, $\hat{x}\,/\,\hat{y}\,/\,\hat{z}$ are unit-vectors in the three cartesian directions, and $n_{x/y/z}$ go from 1 to ∞. In the thermodynamic limit ($L \to \infty$), the one-particle partition function becomes

$$q^{trans} = V\left(\frac{2\pi m k_B T}{h^2}\right)^{3/2} . \tag{10}$$

With this we rewrite the term in brackets in eq. (8) to (employing the ideal gas law $pV = Nk_BT$ and the Stirling formula $\ln N! \approx N \ln N - N$ at some stage)

$$(11) \qquad -\frac{1}{2N}\left[k_BT\ln\left(\frac{1}{N!}(q^{\text{trans}})^N\right) - pV\right] = -\tfrac{1}{2}k_BT\ln\left[\left(\frac{2\pi m}{h^2}\right)^{3/2}\frac{(k_BT)^{5/2}}{p}\right] \quad .$$

Rotational free energy

In the rigid rotator approximation the rotational partition function is written as

$$(12) \qquad q^{\text{rot}} = \sum_{J=0}^{\infty}(2J+1)\exp\left(\frac{-J(J+1)B_o}{k_BT}\right) \quad ,$$

where $B_o = \hbar^2/(2I)$ is the rotational constant and I the moment of inertia depending primarily on mass and equilibrium bond lengths. In case of homonuclear diatomic molecules like O_2 (or other molecules that have multiple indistinguishable orientations), q^{rot} is a bit more tricky as it couples with the nuclear spin degrees of freedom (the total wave function must be antisymmetric under exchange of the indistinguishable particles). At the temperatures of interest to us, this can be approximately combined into a classical symmetry number σ^{sym} indicating the number of indistinguishable orientations that the molecule can have (e.g. =1 for heteronuclear diatomic molecules, =2 for homonuclear diatomic molecules). At such temperatures, where the spacing of the rotational levels is small compared to k_BT, the sum in q^{rot} can be converted into an integral with the Euler-Maclaurin series and one ends up with

$$(13) \qquad \mu^{\text{rot}} \approx -k_BT\ln\left(\frac{k_BT}{\sigma^{\text{sym}}B_o}\right) \quad .$$

Notice that this holds only for linear molecules, where then only B_o enters. In more complex cases one would need to diagonalize the inertial tensor and consider all three eigenvalues A_o, B_o and C_o.

Vibrational free energy

The vibrational contribution is obtained within the harmonic approximation by writing the partition function as a sum over the harmonic oscillators of all M fundamental modes ω_i of the particle,

$$(14) \qquad q^{\text{vib}} = \sum_{i=1}^{M}\sum_{n=0}^{\infty}\exp\left(\frac{-(n+\tfrac{1}{2})\hbar\omega_i}{k_BT}\right) \quad .$$

Evaluation of the geometric series yields

$$(15) \qquad \mu^{\text{vib}} = E^{\text{ZPE}} + \Delta\mu^{\text{vib}} = \sum_{i=1}^{M}\left[\frac{\hbar\omega_i}{2} + k_BT\ln\left(1-\exp\left(\frac{\hbar\omega_i}{k_BT}\right)\right)\right] ,$$

where the first term arises from the zero-point vibrations.

Electronic and nuclear free energy

For most molecules internal excitation energies are large compared to k_BT, so that the only term contributing significantly to the partition function is the ground state. Taking a possible spin degeneracy of

this ground state into account, we end up with

(16) $$\mu^{\text{electr}} \approx E_{O_2}^{\text{total}} - k_B T \ln\left(I^{\text{spin}}\right) \quad ,$$

i.e. with the total energy of the O_2 molecule and a term depending on the electronic spin degeneracy of the ground state, I^{spin}. The same form would also be obtained for the nuclear degrees of freedom, which are even more confined to the ground state due to the much larger separation of nuclear energy levels. Although the nuclear partition function may thus be different from unity (according to the degeneracy of the nuclear spin ground state), we will omit it here, since the nuclear state is rarely altered in chemical processes and therefore does not contribute to the thermodynamic changes discussed here.

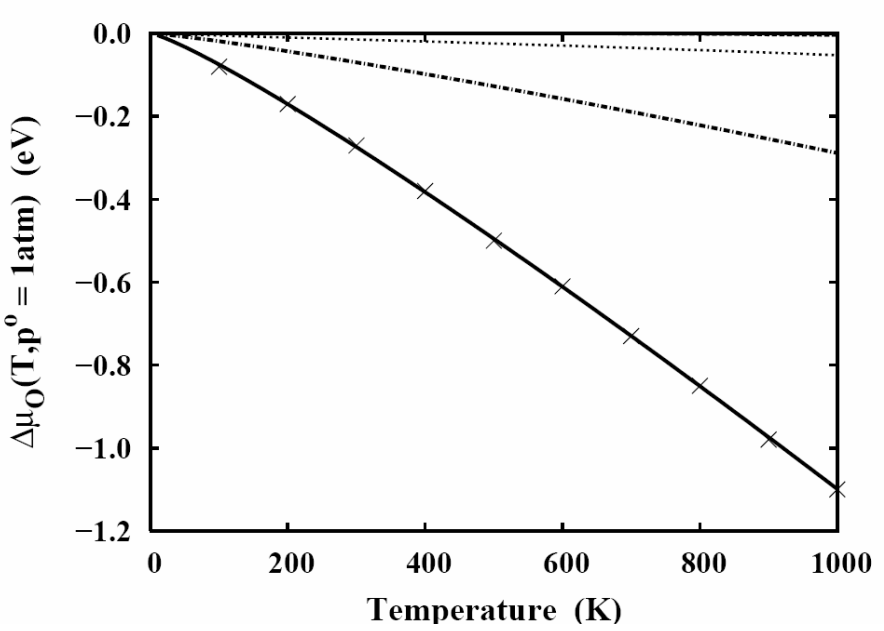

Figure 2: Temperature dependence of the relative oxygen chemical potential $\Delta\mu_O(T,1\text{ atm})$ at p=1 atm. Compared are tabulated values from ref. [23] (crosses) with the result of eq. (18) using the material parameters: σ^{sym}=2, I^{spin}=3, B_o=0.18 meV, and ω_O=196 meV [23]. Additionally shown are the sums of the individual contributions: vibrational (dashed line, almost coinciding with the zero axis), vibrational+nuclear (dotted line), vibrational+nuclear+rotational (dash-dotted line). The remaining large difference to the full result (solid line) is due to the translational contribution.

Bringing it all together

Equations (11), (13), (15), (16) allow the analytic evaluation of the terms entering eq. (8), based on the total energy and vibrational modes of the gas phase molecule, as well as the molecular mass, the rotational constant, the symmetry number and the spin degeneracy (which are available in thermochemical tables [23]). As will become clear below, it is convenient to separate out the total and zero point energy terms and write eq. (8) in the following form

(17) $$\mu_O(T,p) = \tfrac{1}{2} E_{O_2}^{\text{total}} + \tfrac{1}{2} E_{O_2}^{\text{ZPE}} + \Delta\mu_O(T,p) \quad ,$$

where $\Delta\mu_O(T,p)$ contains now all temperature and pressure dependent free energy contributions

$$\Delta\mu_{\mathrm{O}}(T,p) = -\tfrac{1}{2}k_{\mathrm{B}}T\left\{\ln\left[\left(\frac{2\pi m}{h^2}\right)^{3/2}\frac{(k_{\mathrm{B}}T)^{5/2}}{p}\right] + \ln\left(\frac{k_{\mathrm{B}}T}{\sigma^{\mathrm{sym}}B_{\mathrm{o}}}\right) - \ln\left[1-\exp\left(\frac{\hbar\omega_o}{k_{\mathrm{B}}T}\right)\right] + \ln\left(I^{\mathrm{spin}}\right)\right\}. \quad (18)$$

From the structure of eq. (18) it is apparent that one can rewrite eq. (17) in the following form

$$\mu_{\mathrm{O}}(T,p) = \tfrac{1}{2}E_{\mathrm{O_2}}^{\mathrm{total}} + \tfrac{1}{2}E_{\mathrm{O_2}}^{\mathrm{ZPE}} + \Delta\mu_{\mathrm{O}}(T,p^0) + \tfrac{1}{2}k_{\mathrm{B}}T\ln\left(\frac{p}{p^0}\right) \quad , \quad (19)$$

which allows to use tabulated enthalpy and entropy values at standard pressure p^0=1atm [23] to determine $\Delta\mu_{\mathrm{O}}(T,p)$ instead of using eq. (18) [13]. For oxygen, both approaches yield virtually identical results in the temperature range discussed here, as illustrated in Fig. 2 for $\Delta\mu_{\mathrm{O}}(T,1$ atm). However, for other (more complex) molecules one or the other approach may be more convenient, depending on the availability of the gas phase data.

2.2.2 Gibbs free energy of solid bulk and surface

Similar to the procedure applied for the gas phase chemical potential we address the computation of the solid phase Gibbs free energies by first decomposing them into several contributing terms [13,15]

$$G = E^{\mathrm{total}} + F^{\mathrm{vib}} + F^{\mathrm{conf}} + pV \quad , \quad (20)$$

where E^{total} is the total (internal) energy, F^{vib} the vibrational free energy, and F^{conf} the configurational free energy. A crucial aspect that governs our analysis of all of these terms is that the quantities of interest to us, namely surface free energies or Gibbs free energies of adsorption, do not depend on absolute Gibbs free energies. What enters into the corresponding eqs. (3) or (5) are *differences* of Gibbs free energies only. This can allow for quite some degree of error cancellation, in particular if the different terms correspond to rather similar situations like the Gibbs free energies of solid bulk and solid surface.

The dominant term in eq. (20) is the total energy, which as discussed in the introduction is provided through the DFT calculations. We note in passing that the thermodynamic formalism is, of course, general and would be equally valid when using total energies coming from e.g. less accurate schemes. However, when using say a semi-empirical potential to provide the total energies, the accuracy of the ensuing thermodynamic reasoning would also only be at this level. It is precisely the idea of *ab initio* atomistic thermodynamics to carefully evaluate the total energy contributions and thereby carry over the predictive power of the first-principles technique to finite (T,p)-conditions.

Turning to the other terms in eq. (20), we find from a simple dimensional analysis that its contribution to the surface free energy (normalized to unit surface area) will be $[pV/A]$ = atm Å^3/Å^2 ~ 10^{-3} meV/Å^2. Even for p ~ 100 atm, the pV-contribution will therefore still be less than ~0.1 meV/ Å^2. We will see below that in the intended application to metal surfaces in contact with realistic environments this is a negligible contribution compared to the other free energy terms, which are of the order of tens of meV/ Å^2.

The contribution from the vibrational degrees of freedom can be handled with the same harmonic approximation applied already for the gas phase chemical potential. However, instead of writing the vibrational free energy as arising from a sum of discrete fundamental modes ω_i, cf. eq. (15), we now introduce the phonon density of states (DOS) $\sigma(\omega)$ and obtain

$$F^{\mathrm{vib}} = \int d\omega\, F^{\mathrm{vib}}(T,\omega)\,\sigma(\omega) \quad , \quad (21)$$

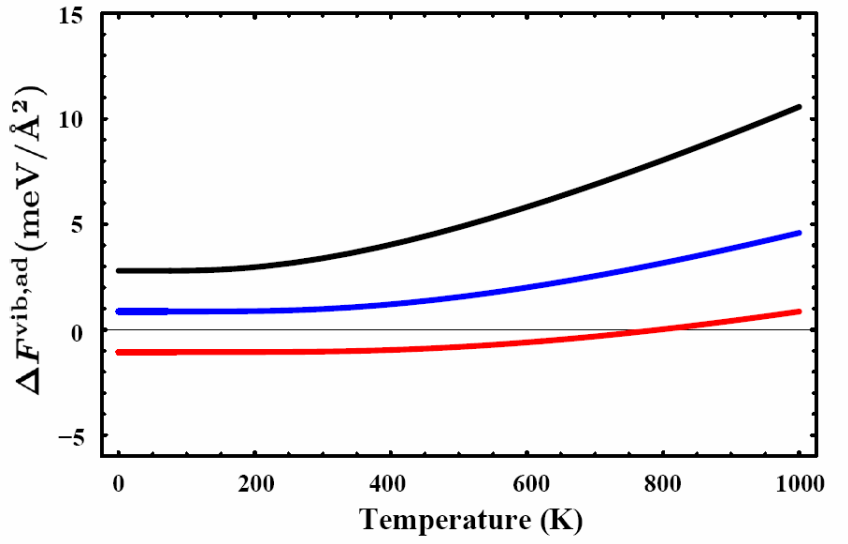

Figure 3: Estimated vibrational contribution $\Delta F^{vib,ad}$ to the Gibbs free energy of adsorption for the *p*(2x2) O/Pd(100) structure. Used is the Einstein approximation to the phonon density of states, where the characteristic frequency of O atoms is changed from 196 meV in the gas phase to 40 meV (black line), 80 meV (blue line) or 120 meV (red line) at the surface. Changes of the vibrational modes of surface Pd atoms upon O adsorption are neglected.

with

$$F^{\mathrm{vib}}(T,\omega) = \frac{\hbar\omega}{2} + k_{\mathrm{B}}T \ln\left(1 - \exp\left(\frac{\hbar\omega}{k_{\mathrm{B}}T}\right)\right) \quad . \tag{22}$$

A proper evaluation of the vibrational contribution to ΔG^{ad} or γ amounts therefore to computing the phonon DOS of the solid bulk and surface. This information is contained in the PES and can correspondingly be calculated by DFT [5]. However, since surface phonon DOS calculations are computationally still quite involved, getting away with simpler approximations would be particularly worthwhile. For this, we come back to the afore mentioned cancellation in the differences of Gibbs free energies. It is crucial to realize that the vibrational free energy of the solid bulk and surface is not small or negligible, yet what matters for the determination of e.g. the Gibbs free energy of adsorption is only the following difference

$$\begin{aligned} &\Delta F^{\mathrm{vib,ad}}(T) \\ &= -\frac{1}{A}\left\{\left[\int d\omega\left(\sigma(N_{\mathrm{O}},N_{\mathrm{M}},\omega) - \sigma_{\mathrm{clean}}(0,N'_{\mathrm{M}},\omega) - \left(N_{\mathrm{M}} - N'_{\mathrm{M}}\right)\sigma_{\mathrm{M}}(\omega)\right)F^{vib}(T,\omega)\right] - \frac{N_{\mathrm{O}}}{2}\mu^{\mathrm{vib}}_{\mathrm{O}_2}(T)\right\} \approx \\ &\approx -\frac{1}{A}\left\{\left[\int d\omega\left(\sigma(N_{\mathrm{O}},N_{\mathrm{M}},\omega) - \sigma_{\mathrm{clean}}(0,N_{\mathrm{M}},\omega) - \left(N_{\mathrm{M}} - N'_{\mathrm{M}}\right)\sigma_{\mathrm{M}}(\omega)\right)F^{vib}(T,\omega)\right] - \frac{N_{\mathrm{O}}}{2}E^{\mathrm{ZPE}}_{\mathrm{O}_2}\right\} \quad , \end{aligned} \tag{23}$$

where σ is the phonon DOS of the surface considered, σ_{clean} the one of the corresponding clean surface, σ_{M} the one of the metal bulk, and in the second line we have realized that the temperature dependent vibrational contribution to $\mu^{\mathrm{vib}}_{\mathrm{O}_2}(T)$ is negligible, cf. Fig. 2. Equation (23) shows that only the changes in the vibrational properties of the atoms at the surface compared to their counterparts in the clean surface, the solid bulk or the gas phase are decisive. Before initiating a full-blown surface phonon DOS

calculation, it can therefore be very valuable to use approximations to σ, σ_{clean}, and σ_M, and obtain an order of magnitude estimate of $\Delta F^{vib,ad}$ first [13]. A very simple approximation would e.g. be an Einstein model, which considers only one characteristic frequency for each atom type. Allowing this frequency to change significantly for surface atoms compared to those in the solid bulk or in the gas phase provides then a first idea of the magnitude of the vibrational contribution. This approach is exemplified in Fig. 3 for the below discussed case of a Pd(100) surface in contact with an oxygen environment. Even for quite extensive variations of the characteristic vibrational modes, the resulting $\Delta F^{vib,ad}$ always stays within $\approx \pm 5$ meV/ Å^2 for the entire temperature range up to 600 K that is of interest to our study. Comparing with the much larger contribution from the total energy terms, we will use this information to justify neglecting the vibrational $\Delta F^{vib,ad}$ below. However, we stress that this is not a general result. There might well be applications where the inclusion of vibrational effects on the surface free energy or Gibbs free energy of adsorption can be important as e.g. in the adsorption of larger molecules [24] or in hydrogen containing environments [25]. In such cases, it may already be sufficient to only consider some prominent vibrational modes, but eventually an explicit calculation of the surface and bulk phonon DOS may be required.

This leaves as remaining term the configurational free energy. A full evaluation of this contribution is computationally most involved, since it requires a proper sampling of the huge configuration space spanned by all possible surface structures. Although modern statistical mechanics methods like Monte Carlo simulations [26,27] are particularly designed to efficiently fulfill this purpose, they still require a prohibitively large number of free energy evaluations to be directly linked with electronic structure theories [6]. A way to circumvent this problem is to map the real system somehow onto a simpler, typically discretized model system, the Hamiltonian of which is sufficiently fast to evaluate. Obvious uncertainties of this approach are how appropriate the model system represents the real system, and how its parameters can be determined from the first-principles calculations. The advantage, on the other hand, is that such a detour via an appropriate ("coarse-grained") model system often provides deeper insight and understanding of the ruling mechanisms. If the considered problem can be described by a lattice defining e.g. the possible adsorption sites for the gas phase species in the system, a prominent example for such a mapping approach comes under the names lattice-gas Hamiltonians (LGHs) or cluster expansions (CEs) [6,28-30].

Here, we will instead concentrate on a much simpler alternative, which focuses on screening a number of known (or possibly relevant) ordered surface structures by directly comparing which of them turns out to be most stable under which (T,p)-conditions, i.e. which of them exhibits the lowest surface free energy or Gibbs free energy of adsorption. For sufficiently low temperatures, the remaining configurational entropy per surface area is then only due to a limited number of defects in these ordered structures and can be estimated as

$$\frac{TS^{conf}}{NA} = \frac{k_B T}{NA} \ln\left(\frac{(N+n)!}{N!n!}\right) \quad , \tag{24}$$

where n is the small number of defects in a system with N surface sites ($n << N$). For N, $n >> 1$ we can apply the Stirling formula which leads to

$$\frac{TS^{conf}}{NA} = \frac{k_B T}{A}\left[\ln\left(1+\frac{n}{N}\right)+\left(\frac{n}{N}\right)\ln\left(1+\frac{N}{n}\right)\right] < 0.34\frac{k_B T}{A} \qquad \left(\forall\, n/N < 10\%\right) \quad . \tag{25}$$

With a typical area per surface site of $A \sim 10$ Å^2 for transition metal surfaces, we correspondingly deduce that the configurational entropy contribution to the Gibbs free energy is less than 3 meV/ Å^2 for any $T <$ 1000 K [15]. We will see below that in the application to a Pd surface in contact with an oxygen environment this is almost always negligible and will qualify to which changes its explicit consideration will lead. While the effect of configurational entropy due to disorder is therefore not of much concern, the

obvious limitation in this direct screening approach is that its reliability is restricted to the number of considered configurations, or in other words that only the stability of those structures plugged in can be compared. The predictive power extends therefore only to those structures that are directly considered, i.e. the existence of unanticipated surface geometries or stoichiometries cannot be predicted. As such, appropriate care should be in place when addressing systems where only limited information about the surface structures is available. With this in mind, the direct screening approach to *ab initio* atomistic thermodynamics can still be a particularly valuable tool, since it allows, for example, to rapidly compare the stability of newly devised structural models against existing ones. In this way, it gives tutorial insight into what structural motives may be particularly important, which may even yield ideas about other structures that one should test as well. Still, the limited reliability to the set of actually considered structural models must always be borne in mind and can really only be overcome by a proper sampling of configurational space, which then leads also to a more general and systematic way of treating phase coexistence and order-disorder transitions.

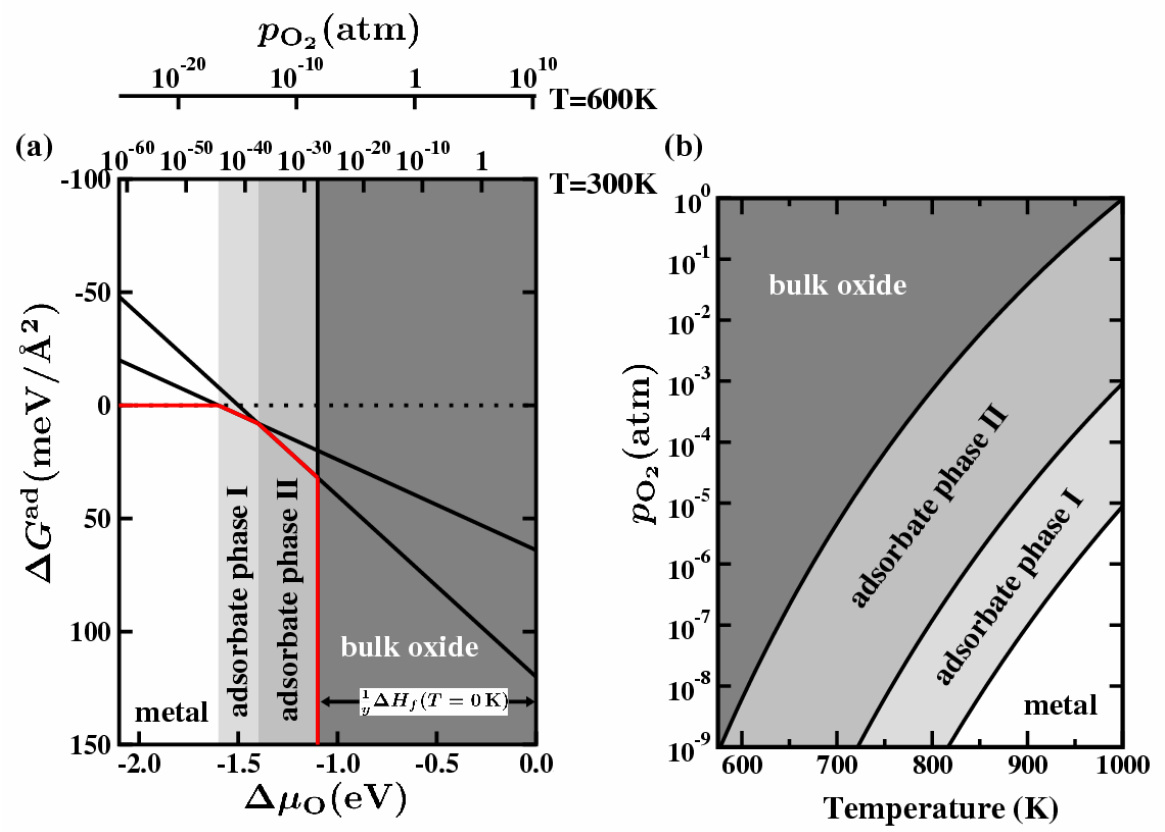

Figure 4: Generic free energy plot (a) and surface phase diagram (b) for a surface in equilibrium with a surrounding oxygen gas phase. a) An adsorbate phase will become more stable than the zero reference clean metal surface, if its ΔG^{ad} >0 for some oxygen chemical potential (note the inverted y-scale!). If there is more than one adsorbate phase, always the one with the largest ΔG^{ad} will become most stable, as indicated here by the red line. Finally, for $\Delta\mu_O > 1/y\ \Delta H_f(T{=}0\mathrm{K})$, the bulk oxide will always result as the most stable phase. b) Converting the obtained $\Delta\mu_O$ stability range for each phase (indicated schematically by the different shaded regions in the free energy plot on the left) into (*T,p*)-conditions using eq. (18) allows to draw the resulting surface phase diagram.

2.3 Free energy plots and surface phase diagrams

We will now employ the general thermodynamic framework developed in sections 2.1 and 2.2 to investigate the structure and composition of a solid surface in contact with a given environment at finite temperature and pressure. More specifically, we aim at applying it to describe a single-crystal transition metal surface in contact with an oxygen gas phase, but before we address the actual case of a Pd(100) surface below let us first spend some time with more general considerations. In light of the discussion in section 2.2.2 we will neglect the vibrational contribution $\Delta F^{\mathrm{vib,ad}}$ to the Gibbs free energy of adsorption, and within the spirit of the direct screening approach we will also neglect the configurational entropy term in the solid phase Gibbs free energies for the time being. This transforms the general eq. (5) into the working equation

$$(26)\quad \Delta G^{\mathrm{ad}}(T,p) \approx -\frac{1}{A}\left(E^{\mathrm{total}}(N_{\mathrm{O}},N_{\mathrm{M}}) - E^{\mathrm{total}}(0,N_{\mathrm{M}}) - \left(N_{\mathrm{M}} - N'_{\mathrm{M}}\right)E_{\mathrm{M}}^{\mathrm{total}} - \frac{N_{\mathrm{O}}}{2}E_{\mathrm{O_2}}^{\mathrm{total}} - N_{\mathrm{O}}\Delta\mu_{\mathrm{O}}(T,p)\right).$$

Evaluating ΔG^{ad} requires now primarily total energies which are directly amenable to electronic structure theory calculations. In the direct screening approach to *ab initio* atomistic thermodynamics, these quantities would be calculated for a number of ordered surface structural models. Equation (26) allows then to directly plot the Gibbs free energy of adsorption for each model as a function of the oxygen chemical potential $\Delta\mu_{\mathrm{O}}$, as illustrated schematically in Fig. 4a. This yields a straight line for each model considered, and at any given $\Delta\mu_{\mathrm{O}}$ the model with the lowest lying line (most stable ΔG^{ad}) is identified as the most stable one under environmental conditions corresponding to this particular oxygen chemical potential. Using eq. (18) in section 2.2.1 allows to relate specific (T,p)-conditions to this chemical potential, and this information can e.g. be included in graphs like Fig. 4a in form of additional x-axes, which give the pressure dependence at some specific temperature. Alternatively, one can concentrate only on the most stable structures, convert the range of chemical potential in which each is most stable into corresponding (T,p) ranges, and plot these stability ranges in surface phase diagrams of the form of Fig. 4b. It is important to realize that both kinds of plots are based on exactly the same information. Surface phase diagrams (Fig. 4b) provide a more direct insight to the experimentally accessible (T,p) conditions, whereas free energy plots (Fig. 4a) summarize the two-dimensional dependence conveniently in the one-dimensional, but less intuitive dependence on the chemical potential. Additionally, it is only in the latter kind of plots that also information about the energetic difference to alternative, less stable surface structural models is provided. These plots make also immediately apparent that the transition from one stable phase to another occurs within the present framework always at a specific value of the oxygen chemical potential, cf. Fig. 4a, which is the reason why the phase boundaries in (T,p) surface phase diagrams of the type of Fig. 4b exhibit similar curvatures (lines of constant $\Delta\mu_{\mathrm{O}}$) . We note in passing that a third and equally equivalent way of plotting the results would be to plot the stability ranges in (*1/T, p*)-figures, in which case these boundaries between the stable phases would then result as straight lines [31].

Realizing that the definition for the average binding energy at $T = 0$ K is

$$(27)\qquad E_b = -\frac{1}{N_{\mathrm{O}}}\left(E^{\mathrm{total}}(N_{\mathrm{O}},N_{\mathrm{M}}) - E^{\mathrm{total}}(0,N_{\mathrm{M}}) - \frac{N_{\mathrm{O}}}{2}E_{\mathrm{O_2}}^{\mathrm{total}}\right) \quad ,$$

with $E_b > 0$ for exothermicity, we arrive at the expression

$$(28)\qquad \Delta G^{\mathrm{ad}}(T,p) \approx \frac{N_{\mathrm{O}}}{A}E_b + \left(N_{\mathrm{M}} - N'_{\mathrm{M}}\right)E_{\mathrm{M}}^{\mathrm{total}} + \frac{N_{\mathrm{O}}}{A}\Delta\mu_{\mathrm{O}}(T,p) \quad ,$$

which has a rather intuitive structure: Forming the oxidized surface by accommodating N_{O} oxygen atoms yields an energy gain of $N_{\mathrm{O}}E_b$ (per surface area), that is opposed by the cost of taking these O atoms out of

the gas phase reservoir, hence $N_O\Delta\mu_O$. The equivalent term $(N_M - N'_M)E_M^{total}$ comes only into play for oxidized surfaces where the total number of metal atoms is different to the one of the reference clean metal surface, and represents then the cost of transferring the corresponding number of metal atoms to or from the reservoir represented by the metal bulk.

On the basis of eq. (28) the general structure of a surface free energy plot for a metal surface in contact with an oxygen environment can nicely be discussed. In the limit of an infinitely dilute gas ($\Delta\mu_O \rightarrow -\infty$), any surface structure containing oxygen ($N_O \neq 0$) will exhibit an infinitely negative ΔG^{ad}, reflecting that it is very unfavorable to maintain oxygen adsorbed at the surface under such conditions. As intuitively clear, the clean surface will therefore always result as most stable in such environments. With increasing oxygen content in the gas phase, $\Delta\mu_O$ will become less negative and so will the ΔG^{ad} of oxygen containing surface structural models. Eventually, one of them will exhibit a $\Delta G^{ad} > 0$ and will then become more stable than the clean surface. At corresponding oxygen pressures and temperatures, oxygen is getting stabilized at the surface, cf. Fig. 4a, and the governing factors for this are immediately revealed by the structure of eq. (28): The slope of each ΔG^{ad}-line is determined by N_O/A, i.e. the more oxygen is contained in the structure, the faster this structure becomes more favorable with increasing oxygen chemical potential. For surfaces preserving the number of metal atoms ($N_M = N'_M$), the x-axis intercept (i.e. the moment when the structure becomes more stable than the clean surface) is reached at $\Delta\mu_O = -E_b$. A more stable binding of oxygen in the surface structural model will correspondingly shift the ΔG^{ad}-line in the free energy plot down and the x-axis intercept to the left, and will thereby render the structure more stable than the clean surface at already lower oxygen contents in the gas phase. A large ΔG^{ad} at increasing oxygen chemical potential and therewith the chance to become the most stable structure can therefore be reached by surface structural models that either offer a strong binding of their oxygen species or contain a large number of oxygen atoms per surface area. This way, a surface structure that strongly binds a few oxygen atoms could for example become more favorable than the clean surface at low chemical potentials, while another surface structure with weaker binding, but higher oxygen coverage will eventually become more stable at somewhat higher chemical potentials due to its steeper slope, cf. Fig. 4a.

The highest number of oxygen atoms per surface area is ultimately reached by bulk oxide structures, i.e. when the oxygen content in the environment is high enough to create an infinitely thick bulk oxide on top of the metal substrate. Since then $N_O \rightarrow \infty$, the corresponding ΔG^{ad}-line in the free energy plot is vertical, cf. eq. (28). The intercept of this line with the x-axis is given by the condition that the bulk oxide becomes thermodynamically more favorable than an equivalent amount of bulk metal and gas phase oxygen

$$g_{M_xO_y} \leq x g_M + y\mu_O \quad , \tag{29}$$

where $g_{M_xO_y}$ is the Gibbs free energy per formula unit of the oxide bulk. Using eq. (17), this yields

$$\Delta\mu_O \gtrsim \frac{1}{y}\left(g_{M_xO_y}(T,p) - x g_M(T,p) - \frac{y}{2}E_{O_2}^{total} \right) = \frac{1}{y}\Delta H_f(T = 0\text{K}) \quad , \tag{30}$$

where $\Delta H_f(T=0\text{ K})$ is the heat of formation of the bulk oxide at T=0 K [13,17]. For any $\Delta\mu_O$ higher than this limit, the bulk oxide will always be the stable phase, cf. Fig. 4a.

After this more general discussion we proceed with the specific case of a Pd(100) surface in contact with an oxygen atmosphere, to illustrate how the direct screening approach to *ab initio* atomistic thermodynamics works and what it can contribute in practice. Typical for late transition metal surfaces, the interest in this system comes from the widespread technological use of Pd, for example in the area of oxidation catalysis [32]. Although this material is known for its propensity to form oxidic structures in technologically-relevant high oxygen pressure environments, the possible formation of sub-nanometer thin

oxidic films (so-called surface oxides) has only recently been addressed [17,18,33,35,36]. While traditionally such films were conceived as closely related thin versions of the corresponding (known) bulk oxides, recent atomic-scale characterizations of initial few-atomic-layer thick oxide overlayers especially on Pd and Ag surfaces have revealed structures that have little resemblance to their bulk counterparts, and/or are influenced to a large degree by a strong coupling to the underlying metal substrate [17,19,20,33-37]. Due to this coupling and structures particularly suited for layered configurations, one may expect the stability range for such surface oxides to exceed that of the hitherto discussed bulk oxides [18].

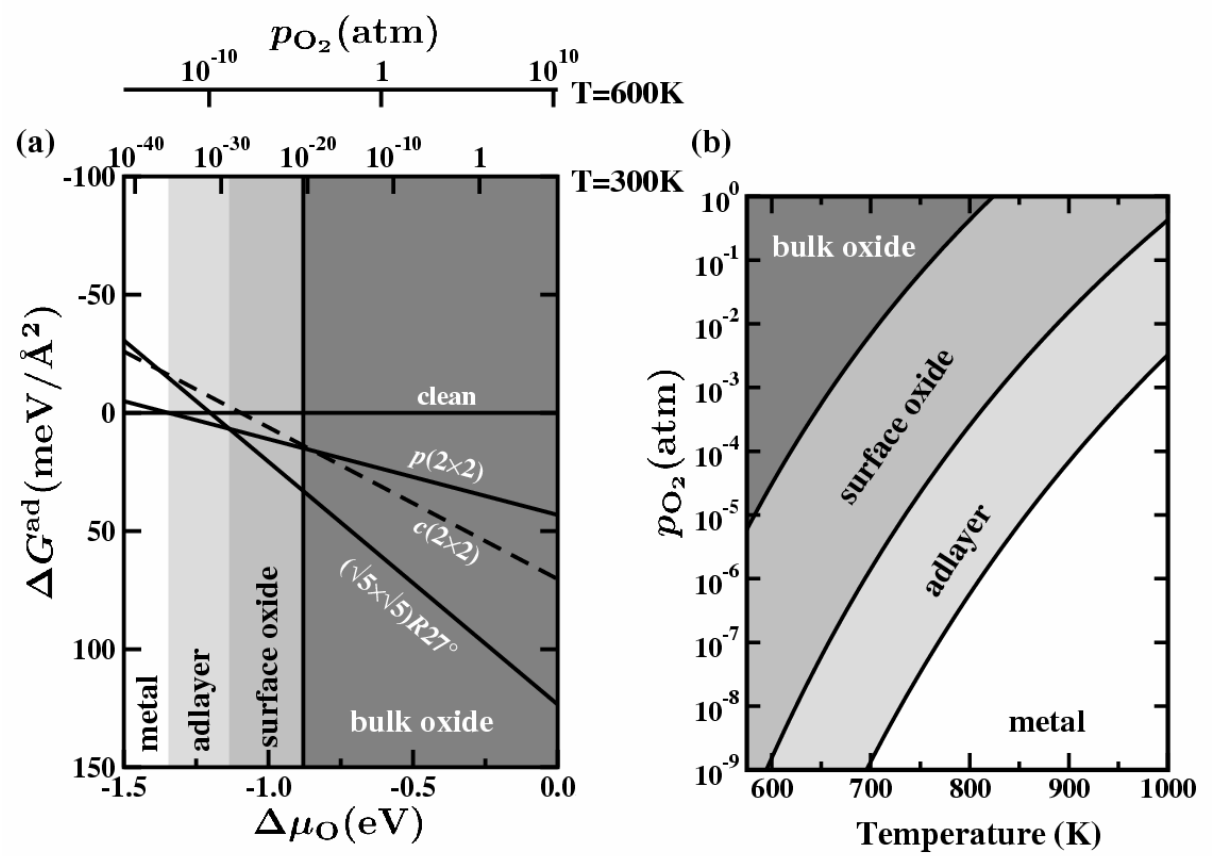

Figure 5: Computed free energy plot (a) and surface phase diagram (b) for O/Pd(100), following the general style of Fig. 4. Considered are two ordered adlayers with O in the fourfold hollow sites (*p*(2x2), ¼ monolayer (ML) coverage, and *c*(2x2), ½ ML coverage) and the (√5 x √5)*R*27°–O surface oxide (0.8 ML coverage). Note the extended stability range of the surface oxide compared to the known PdO bulk oxide. The total energies (DFT-GGA, PBE) used to construct this graph via eq. (26) are taken from refs. [36,40], the surface unit-cell area of Pd(100) is 7.8 Å^2.

In the spirit of the direct screening approach we therefore consider here the three experimentally characterized oxygen-containing surface structures to date, namely two ordered adlayers with O in the fourfold hollow sites (*p*(2x2), ¼ monolayer (ML) coverage, and *c*(2x2), ½ ML coverage) and the (√5 x √5)*R*27°–O surface oxide (0.8 ML coverage) [38,39]. The latter structure corresponds to a rumpled, but commensurate PdO(101) film with a strong coupling to the underlying substrate [35]. Evaluating the calculated DFT binding energies for these three surface structures leads to the results displayed in Fig. 5a [35,36,40]. They nicely follow the more general structure discussed above: While the clean surface is the most stable structure at the lowest oxygen chemical potentials, the *p*(2x2) structure exhibits a higher ΔG^{ad}

for $\Delta\mu_O > -1.35$ eV. Due to its steeper slope (higher coverage), the ($\sqrt{5}$ x $\sqrt{5}$)*R*27°–O surface oxide becomes even more favorable for $\Delta\mu_O > -1.15$ eV, while ultimately in the most oxygen-rich environments ($\Delta\mu_O > -0.87$ eV) the PdO bulk oxide results as most stable phase. Converting this information about the stability ranges of these different phases by means of eq. (18) into (*T,p*)-conditions leads to the plot also shown in Fig. 5b.

Referring to the more detailed original literature [17,18,35,36], we restrict our discussion of these results here to two noteworthy points: First, as motivated above, there is indeed a surprisingly large range of (*T,p*)-conditions, where the surface oxide structure represents the thermodynamically most stable structure. In corresponding oxygen environments, this sub-nanometer thin film will thus eventually form on time scales set by possible kinetic limitations, but never grow thicker. Due to this finite thickness, the coupling at the oxide-metal interface and an atomic structure that can be quite different to the one of the known bulk oxides, one might suspect new properties that are distinct to those of surfaces of both bulk metals and bulk oxides, and could thus be of potential interest for applications. Second, the *c*(2x2) structure is never a most stable phase. This implies that the frequent observation of this structure in ultra-high vacuum (UHV) experiments [38,39] is a mere outcome of the limited O supply offered, as well as of kinetic barriers to the formation of the surface oxide, e.g. due to limitations in the O penetration at the low temperatures employed (UHV experiments are typically performed by depositing a finite number of adatoms, rather than by maintaining a given gas pressure [41]).

Instead of further dwelling on the physics of this system, let's return now to the methodological discussion. As already stated several times, the validity of these results is restricted by the limited number of surface structural models considered in the direct screening approach. Apart from that, uncertainties are introduced due to the neglected vibrational free energy contribution to ΔG^{ad}, as well as due to inaccuracies in the total energy *difference* entering eq. (26). Inspecting the *y*-axis scale of the free energy plot in Fig. 5a, we see for example that even small changes in ΔG^{ad} of the order of ~ ±5 meV/ Å^2 may still considerably shift the (*T,p*) stability ranges for the various phases (due to the shifted crossing points of the various lines with different, but similar slopes). On the other hand, the sequence of stable phases in increasingly oxygen-rich environments (clean surface, *p*(2x2) adlayer, ($\sqrt{5}$ x $\sqrt{5}$)*R*27°–O surface oxide, PdO bulk oxide) is not affected by such changes [40]. Both the numerical uncertainty in the total energy difference due to the finite basis set employed in the DFT calculations and the neglected $\Delta F^{vib,ad}$ term are of this order of magnitude and in the corresponding light the reported results have to be seen. An even larger uncertainty in the total energy difference may result from the approximate exchange-correlation (XC) functional in the DFT calculations. While in the present example using local-density or several generalized gradient functionals still led to the same sequence of stable phases [40], extreme caution is advisable in general. As always, the accuracy level is dictated by the questions one wants to get answered. If required, systematic improvement on the numerical uncertainty in the total energy difference and on the vibrational free energy contribution is in principle always possible (albeit in practice at possibly high or prohibitive computational cost). Concerning the uncertainty due to the approximate XC functional, at least one may compare the results obtained with differently constructed functionals. If doubts remain, a regional XC correction or higher-level electronic structure calculations may be necessary.

As a final point, we briefly comment on the effect of the neglected configurational entropy contribution. As discussed in section 2.2.2 at sufficiently low temperatures this term is quite small and can therefore only have an effect when two competing ΔG^{ad}-lines come very close to each other [15]. This is the case at the transitions between stable phases, and in fact, the deliberately neglected configurational entropy term is the reason why these boundaries are drawn abrupt in the surface phase diagram in Fig. 5 – even at the highest temperatures shown. In reality, finite phase coexistence regions should occur at finite temperatures, i.e. regions in which with changing pressure one phase gradually becomes populated and the other one depopulated. With increasing temperature, the width of these coexistence regions around the phase transitions increases, until eventually there are no pressures left in which one still finds the well-ordered surface structures now displayed in Fig. 5. Only a proper evaluation of the configurational entropy

term, e.g. through Monte Carlo simulations, can provide detailed insight into these order-disorder transitions and/or the phase coexistence regions themselves, and corresponding care has to be taken in the interpretation of results at elevated temperatures, when the configurational entropy term is neglected as in the direct screening approach to *ab initio* atomistic thermodynamics discussed here [6].

3.0 SUMMARY

A predictive modeling of materials properties requires a consistent treatment in the wide hierarchy of scales from the electronic level to macroscopic lengths and times. The central idea of *ab initio* atomistic thermodynamics is to employ the information on the potential energy surface provided by modern electronic structure theories, in order to calculate appropriate thermodynamic potential functions. With the latter, macroscopic system properties at finite temperatures can immediately be discussed. At surfaces, such a thermodynamic description can be particularly useful, since it provides the possibility to suitably divide the total system into smaller subsystems that are mutually (or partly) in equilibrium with each other. This way, infinite, but homogeneous parts of the system like bulk or surrounding gas phase can be efficiently represented by corresponding reservoirs, which e.g. allows to address surfaces in contact with realistic environments.

In this tutorial text we have focused on a very simple realization of this general scheme, namely the direct screening approach, to determine the equilibrium geometry and composition of a solid surface in contact with a given environment at finite temperature and pressure. For the sake of clarity we considered the case of a monoatomic metal and an oxygen atmosphere, but the conceptual framework is readily generalized to more complex systems, involving compounds like oxides or alloys, or environments containing multiple gas phase species. In the direct screening approach one focuses on a number of known (or possibly relevant) ordered surface structures, and directly compares which of them turns out to be most stable under which (T,p)-conditions, i.e. which of them exhibits the lowest surface free energy or Gibbs free energy of adsorption. This provides first valuable insight into the structure and composition of the surface in realistic or technologically relevant environments at virtually no extra computational cost compared to the underlying electronic structure theory calculations.

The major limitation of the direct screening approach is that its reliability is restricted to the number of considered configurations, i.e. the existence of unanticipated surface geometries or stoichiometries cannot be predicted. This can only be overcome by a proper sampling of configurational space, as e.g. provided by modern statistical mechanics methods like Monte Carlo simulations, which then leads also to a more general and systematic way of treating phase coexistence and order-disorder transitions. Last, not least, one should always keep in mind that (regardless of whether direct screening or statistical sampling) *ab initio* atomistic thermodynamics is – as reflected by the name – a thermodynamic theory and as such describes systems that had infinitely long time to fully equilibrate. It provides no information on what time scale (with which kinetic hindrance) this equilibration took place. For this, one necessarily needs to go beyond a thermodynamic description and explicitly follow the kinetics of the system over time.

Acknowledgments

We gratefully acknowledge valuable discussions and contributions from our (former) colleagues at the Theory Department of the Fritz-Haber-Institut, in particular Wei-Xue Li, Cathy Stampfl and Mira Todorova. Particular thanks go to Matthias Scheffler for his continued support and the many insightful discussions that led to the development and application of the here described *ab initio* atomistic thermodynamics approach to metal oxidation and oxide formation. This work was partially supported by the Deutsche Forschungsgemeinschaft (DFG) in the priority program SPP-1091, and by the EU under contract no. NMP3-CT-2003-505670 ($NANO_2$).

4.0 REFERENCES

[1] P. Hohenberg and W. Kohn, Phys. Rev. B **136**, 864 (1964).

[2] W. Kohn and L. Sham, Phys. Rev. A **140**, 1133 (1965).

[3] R.G. Parr and W. Yang, *Density Functional Theory of Atoms and Molecules*, Oxford University Press, New York (1989).

[4] R.M. Dreizler and E.K.U. Gross, *Density Functional Theory*, Springer, Berlin (1990).

[5] R.M. Martin, *Electronic Structure. Basic Theory and Practical Methods*, Cambridge University Press, Cambridge (2004).

[6] K. Reuter, C. Stampfl, and M. Scheffler, "Ab Initio Thermodynamics and Statistical Mechanics of Surface Properties and Functions". In: S. Yip (ed.), *Handbook of Materials Modeling, Part A. Methods*, Springer, Berlin (2005). ISBN-10 1-4020-3287-0.

[7] C.M. Weinert and M. Scheffler, In: H.J. von Bardeleben (ed.), *Defects in Semiconductors*, Mat. Sci. Forum **10-12**, 25 (1986).

[8] E. Kaxiras, Y. Bar-Yam, J.D. Joannopoulos, and K.C. Pandey, Phys. Rev. B **35**, 9625 (1987).

[9] M. Scheffler, "Thermodynamic Aspects of Bulk and Surface Defects – First-Principles Calculations". In: J. Koukal (ed.), *Physics of Solid Surfaces – 1987*, Elsevier, Amsterdam (1988); M. Scheffler and J. Dabrowski, Phil. Mag. A **58**, 107 (1988).

[10] G.-X. Qian, R.M. Martin, and D.J. Chadi, Phys. Rev. B **38**, 7649 (1988).

[11] X.-G. Wang, W. Weiss, Sh.K. Shaikhutdinov, M. Ritter, M. Petersen, F. Wagner, R. Schlögl, and M. Scheffler, Phys. Rev. Lett. **81**, 1038 (1998).

[12] X.-G.Wang, A. Chaka, and M. Scheffler, Phys. Rev. Lett. **84**, 3650 (2000).

[13] K. Reuter and M. Scheffler, Phys. Rev. B **65**, 035406 (2002).

[14] K. Reuter and M. Scheffler, Phys. Rev. Lett. **90**, 046103 (2003).

[15] K. Reuter and M. Scheffler, Phys. Rev. B **68**, 045407 (2003).

[16] Z. Lodzianan and J.K. Nørskov, J. Chem. Phys. **118**, 11179 (2003).

[17] K. Reuter and M. Scheffler, Appl. Phys. A **78**, 793 (2004).

[18] K. Reuter, "Nanometer and Sub-Nanometer Thin Oxide Films at Surfaces of Late Transition Metals". In: U. Heiz, H. Hakkinen, and U. Landman (eds.), *Nanocatalysis: Principles, Methods, Case Studies*, Springer, Berlin (2006).

[19] W.-X. Li, C. Stampfl, and M. Scheffler, Phys. Rev. B **68**, 16541 (2003).

[20] W.-X. Li, C. Stampfl, and M. Scheffler, Phys. Rev. Lett. **90**, 256102 (2003).

[21] J.R. Kitchin, K. Reuter, and M. Scheffler, Phys. Rev. B (in preparation).

[22] D.A. Mc Quarrie, *Statistical Mechanics*, Harper and Row, New York (1976).

[23] D.R. Stull and H. Prophet, *JANAF Thermochemical Tables*, 2nd edn., U.S. National Bureau of Standards, Washington, D.C. (1971).

[24] D. Loffreda, Surf. Sci. (in press).

[25] Q. Sun, K. Reuter, and M. Scheffler, Phys. Rev. B **67**, 205424 (2003).

[26] D. Frenkel and B. Smit, *Understanding Molecular Simulation*, 2nd edn., Academic Press, San Diego (2002).

[27] D.P. Landau and K. Binder, *A Guide to Monte Carlo Simulations in Statistical Physics*, Cambridge University Press, Cambridge (2002).

[28] D. de Fontaine, In: P.E.A. Turchi and A. Gonis (eds.), *Statics and Dynamics of Alloy Phase Transformations*, NATO ASI Series, Plenum Press, New York (1994).

[29] J.M. Sanchez, F. Ducastelle, and D. Gratias, Physica A **128**, 334 (1984).

[30] A. Zunger, "First Principles Statistical Mechanics of Semiconductor Alloys and Intermetallic Compounds". In: P.E.A. Turchi and A. Gonis (eds.), *Statics and Dynamics of Alloy Phase Transformations*, NATO ASI Series, Plenum Press, New York (1994).

[31] C.T. Campbell, Phys. Rev. Lett. (in press).

[32] G. Ertl, H. Knözinger, and J. Weitkamp (eds.), *Handbook of Heterogeneous Catalysis*, Wiley, New York (1997).

[33] E. Lundgren, G. Kresse, C. Klein, M. Borg, J.N. Andersen, M. De Santis, Y. Gauthier, C. Konvicka, M. Schmid, and P. Varga, Phys. Rev. Lett. **88**, 246103 (2002).

[34] A. Michaelides, M.L. Bocquet, P. Sautet, A. Alavi, and D.A. King, Chem. Phys. Lett. **367**, 344 (2003).

[35] M. Todorova, E. Lundgren, V. Blum, A. Mikkelsen, S. Gray, J. Gustafson, M. Borg, J. Rogal, K. Reuter, J.N. Andersen, and M. Scheffler, Surf. Sci. **541**, 101 (2003).

[36] E. Lundgren, J. Gustafson, A. Mikkelsen, J.N. Andersen, A. Stierle, H. Dosch, M. Todorova, J. Rogal, K. Reuter, and M. Scheffler, Phys. Rev. Lett. **92**, 046101 (2004).

[37] A. Michaelides, K. Reuter, and M. Scheffler, J. Vac. Sci. Technol. A **23**, 1487 (2005).

[38] D. Kolthoff, D. Jürgens, C. Schwennicke, and H. Pfnür, Surf. Sci. **365**, 374 (1996).

[39] G. Zheng and E.I. Altman, Surf. Sci. **504**, 253 (2002).

[40] J. Rogal, K. Reuter, and M. Scheffler (in preparation).

[41] D.P. Woodruff and T.A. Delchar, *Modern Techniques of Surface Science*, 2nd edn., Cambridge University Press, Cambridge (1994).